Journal of Nuclear Materials 403 (2010) 48–61

Contents lists available at ScienceDirect

Journal of Nuclear Materials

journal homepage: www.elsevier.com/locate/jnucmat

Thermophysical and mechanical properties of near-stoichiometric fiber CVI SiC/SiC composites after neutron irradiation at elevated temperatures

Yutai Katoh *, Lance L. Snead, Takashi Nozawa, Sosuke Kondo, Jeremy T. Busby

Materials Science and Technology Division, Oak Ridge National Laboratory, P.O. Box 2008, Oak Ridge, TN 37831-6138, United States

ARTICLE INFO

Article history:
Received 21 October 2009
Accepted 1 June 2010

ABSTRACT

Thermophysical and mechanical properties of high purity chemically vapor-deposited (CVD) SiC and chemically vapor-infiltrated SiC matrix, pyrocarbon/SiC multilayered interphase composites with Hi-Nicalon™ Type-S and Tyranno™-SA3 SiC fibers were evaluated following neutron irradiation. Specimens including statistically significant population of tensile bars were irradiated up to 5.3 displacement-per-atom at ~220 to ~1080 °C in the Advanced Test Reactor at Idaho National Laboratory and High Flux Isotope Reactor at Oak Ridge National Laboratory.

Thermal diffusivity/conductivity of all materials decreased during irradiation. The reciprocal thermal diffusivity linearly increased with temperature from ambient to the irradiation temperature. The magnitude of defect thermal resistance was distinctively different among materials and its ranking was Hi-Nicalon™ Type-S > Tyranno™-SA3 > CVD SiC regardless of irradiation condition. Dynamic Young's modulus decrease for the irradiated CVD SiC exhibited explicit correlation with swelling. No significant effects of neutron irradiation on tensile properties of the composites were revealed, except for an anomaly case for the Hi-Nicalon™ Type-S composite irradiated in a specific condition. According to the single filament tensile evaluation, fibers of both types retained the original strength during irradiation at intermediate temperatures but significantly deteriorated during bare fiber irradiation at ~910 °C. However, fiber strength deterioration was not observed when irradiated in composite form. Irradiation effects on the fiber–matrix interface properties were discussed based on results from the composite and single filament tensile tests, the hysteresis analysis, and the fracture surface examination.

1. Introduction

Silicon carbide (SiC) ceramics are considered attractive for applications to nuclear services for their outstanding features including elevated temperature strength, chemical inertness, stability in radiation environments, and low activation/low decay heat properties [1,2]. SiC-based materials in forms of continuous fiber composites (continuous SiC fiber-reinforced SiC-matrix composites; SiC/SiC composites) provide additional advantages such as improved reliability, ability to fabricate large complex-shaped components, and ability to anisotropically tailor various properties to meet the design requirements [3,4]. The improved reliability of the composite form comes from the insensitivity of strength properties to surface or internal flaws (notch-insensitivity): (1) fracture strength determined by statistical strength properties of the reinforcing fibers (predictability), and (2) very significantly enhanced fracture energy due to friction of sliding fibers bridging finely-deflected matrix micro-cracks (fracture toughness) .

SiC/SiC composites are considered promising or viable materials in various nuclear programs which aim at the development of fusion energy [3], very high temperature gas-cooled thermal reactors [5], gas-cooled fast reactors [6], advanced liquid salt-cooled reactors [7], etc. For these applications, among various high temperature nuclear materials such as refractory metals and carbon composites, SiC/SiC composites are outstanding in terms of radiation stability, chemical inertness, and reproducibility or ability of quality control. On the other hand, the primary risk factors associated with the attempt to use SiC/SiC composites are the lack of industrial experience, in particular reliability during prolonged services in the extremity of harsh environments, properties database, and design codes for specific applications.

The objective of the present work is to advance understanding of the effects of neutron irradiation at elevated temperatures on properties of chemically vapor-deposited (CVD) high purity SiC and advanced SiC/SiC composites, specifically ones with near-stoichiometric SiC fibers and high purity, chemically vapor-infiltrated (CVI) SiC matrices. One of the emphases was obtaining statistically significant population of data for composite mechanical properties. The neutron irradiation of near-stoichiometric SiC fiber CVI SiC-matrix composite was first irradiated in RB-13 J [8] and rabbit

* Corresponding author. Tel.: +1 865 576 5996; fax: +1 865 241 3650.
E-mail address: katohy@ornl.gov (Y. Katoh).

0022-3115/$ - see front matter © 2010 Elsevier B.V. All rights reserved.
doi:10.1016/j.jnucmat.2010.06.002

capsules [9] in High Flux Isotope Reactor (HFIR), Oak Ridge National Laboratory, and demonstrated the retention of flexural strength after irradiation to ~8 dpa at 350 and 500 °C and ~0.6 dpa at ~400 °C, respectively. Tensile specimens of the similar materials were then irradiated in HFIR RB-14 J [10,11] and Joyo CMIR [12] to doses 6–12 dpa at 300–800 °C. These experiments showed a general lack of irradiation-induced strength deterioration, however, convincing conclusions were not drawn due to significant specimen-to-specimen data scatter. In our previous work, a fairly large number of specimens was tested following irradiation in HFIR rabbit capsules demonstrating minor and non-progressive reduction in flexural strength up to ~3.5 dpa at 300–800 °C [13]. In the present work, statistically significant results of tensile properties evaluation following neutron irradiation up to ~5.3 dpa at up to ~1000 °C are presented and analyzed.

2. Experimental

Materials evaluated were a monolithic CVD SiC and CVI SiC-matrix, woven SiC-fiber composites. The monolithic material was high purity (>99.995%), theoretical density (3.21 g/cm^3) polycrystalline beta-phase SiC produced by Rohm & Haas Advanced Materials.[1] The composite materials were fabricated using two-dimensional (2D) satin-weave fabrics of either Hi-Nicalon™ Type-S (Nippon Carbon Co.,[2] "HNLS" hereafter) or Tyranno™-SA3 (Ube Industries, Ltd.,[3] "SA3" hereafter) near-stoichiometric SiC fibers in the 0°/90° stacking configuration. The matrix was deposited through thermal decomposition of a silane-based precursor by the isothermal, isobaric chemical vapor-infiltration process. A multilayered interphase, consisting of alternating layers of ~20 nm-thick pyrolytic carbon (PyC) and ~100 nm-thick SiC, was deposited in a similar way onto the surface of the woven fabrics. Details of the multilayered interphase are found in the previous paper [13]. Both the interphase deposition and the matrix densification were performed by Hypertherm High-Temperature Composites, Inc.[4] Attributes of the composite materials are summarized in Table 1.

Chemical compositions of the materials as determined by gas discharge mass spectroscopy are summarized in Table 2. Differences between the HNLS and SA3 composites are believed to be caused by different chemistries of the two fiber types, because the interphase and the matrix depositions were performed in identical conditions and the CVI process employed is known to produce high purity SiC matrices with nitrogen as the primary impurity. It is noteworthy that substantial amounts of oxygen, sulfur, and barium are present in the HNLS composite, whereas the SA3 composite contains relatively large amounts of aluminum, boron, and zinc. The ~330 mass-ppm boron in the SA3 composite will produce ~120 at.ppm helium after irradiation. The anticipated effect of helium production is minimal because of the low concentration. The influences of other impurities on irradiation effects in SiC are unknown.

The fabricated composite plates were machined into miniature tensile specimens so that the loading direction was parallel to one of the fiber orientations. The shoulder-loading specimen geometry specially established for neutron irradiation studies by Nozawa et al. was adopted [14]. Dimensions of the miniature specimen's gauge section are 15 mm (l) × 3 mm (w) × 2.3 mm (t). It is reported that the small gauge size causes reduced proportional limit stresses but does not significantly affect other tensile properties [14,15]. A portion of tensile specimens of the HNLS composites were used for a preliminary evaluation, in which: (1) reproducibility of measured tensile properties and (2) influence of the cyclic loading, as compared with the monotonic loading, on tensile properties were examined.

Table 1
Details of composite materials evaluated. Numbers in parentheses indicate standard deviations.

	Hi-Nicalon™ Type-S CVI-SiC composite	Tyranno™-SA3 CVI-SiC composite
Reinforcement		
Fiber type	Hi-Nicalon™ Type-S	Tyranno™-SA Grade 3
Nominal chemistry	$SiC_{1.05}$, 0.2%-O	$SiC_{1.07}$, 0.5%-Al
Fiber diameter	~11 μm	~7.5 μm
Filament/tow	500	1600
Fabric architecture	8-harness satin-weave	8-harness satin-weave
Thread count	22 × 22 TPI	20 × 20 TPI
Interphase	Multilayered interphase 5 × (PyC<20 nm>/SiC <100 nm>)	
Matrix	CVI-SiC	
Composite		
Fiber volume fraction	~31%	~33%
Mass density (g/cm^3)	~2.74	~2.65
Estimated porosity	11%	~12%
Thermal conductivity (W/m-K)		
100 °C	9.4 (1.4)	25.1 (1.0)
500 °C	7.1 (1.1)	18.4 (0.8)
1000 °C	6.0 (1.4)	14.0 (0.7)

Neutron irradiation was performed either in Advanced Test Reactor (ATR, Idaho National Laboratory, Idaho Falls, Idaho) or HFIR. Irradiation vehicles SC-03-1 through 5 were used for the ATR irradiation. Those capsules were irradiated for 292 effective full power days (EFPD), receiving neutron fluences 0.31–5.4 displacement-per-atom (dpa) for SiC. The irradiation temperature for these capsules was passively controlled by the pre-determined gas mixture in the gap between the specimen holders and the capsule housings. In addition to the CVD SiC and the composites, specimens of both types fibers were irradiated. A portion of the CVD SiC specimens were used as the passive temperature monitors. Temperatures at the individual specimen positions during irradiation were estimated based on the calculated temperature distribution within the capsules and using result of the passive thermometry as the calibration points. For the HFIR irradiation, target holder rabbit capsules were irradiated up to ~4.2 dpa in the flux trap position. Irradiation temperatures were determined based on thermal recovery of electrical resistivity using CVD SiC temperature monitor bars.

Tensile tests of the irradiated specimens were carried out at ambient temperature in the cyclic loading mode, upon confirming that the cyclic loading does not impose a noticeable influence on the tensile properties of the materials used. The cyclic loading mode employed was that incorporates repeated unloading/reloading sequences at every incremental peak tensile stress of 25 MPa. By analyzing the unloading/reloading hysteresis loops, additional information related with the matrix crack density and the interfacial frictional stress could be obtained. Other than adopting the cyclic loading, the tensile test procedure followed the general guidelines of ASTM International C1275.

For the CVD SiC specimens, mass density was measured using a density gradient column. Thermal diffusivity was measured with a laser flash instrument and was converted into thermal conductivity values using the heat capacity data from literature [2]. Dynamic Young's modulus was determined for selected specimens of CVD

[1] Woburn, Massachusetts.
[2] Tokyo, Japan.
[3] Ube, Japan.
[4] Huntington Beach, California.

Table 2
Chemical composition of representative composite samples determined by gas discharge mass spectrometry. Unit is in mass parts-per-million unless otherwise shown.

	Rohm & Haas CVD SiC	Hi-Nicalon™ Type-S CVI-SiC composite	Tyranno™-SA3 CVI-SiC composite
Number of samples	1	2	4
N	~90	0.95%	0.65%
O	~10	0.95%	0.28%
S	0.03	0.15%	160
Ba	0.23	600	78
Zn	<0.05	65	290
Al	<0.01	28	490
B	0.46	11	330
Na	0.01	29	120
Cl	0.05	170	130
P	<0.01	13	41
Ca	<0.05	30	33
Mg	<0.01	15	13
Ti	<0.01	2.7	11
Zr	<0.01	7.8	9
Fe	<0.01	39	9
K	<0.05	2	3.6
W	<0.01	0.3	1.5
Ni	0.01	2.5	1.5
Cu	<0.05	0.5	1.2
Sr	<0.01	2.3	1.5
As	<0.05	1.5	1.0
F	<0.5	4.5	<0.5
Cr	<0.1	0.8	<0.5

SiC using the impulse excitation and vibration method, ASTM International C1259.

3. Results

3.1. CVD SiC irradiation effects and thermometry

The irradiation temperature calibrations were carried out based on the as-irradiated mass densitometry, as-irradiated thermal conductivity measurement, and the annealing of thermal diffusivity. In Table 3, results of the temperature calibration are summarized. Among the three methods, densitometry gives the highest accuracy of the measurement itself [16], and there is a one-to-one correspondence between the irradiation temperature and the saturated value of swelling at below ~1000 °C [2]. Result of the densitometry is given in Table 4. The estimates from the irradiated thermal conductivity agreed very well with the estimates from the densitometry, as expected from the general correspondence between swelling and thermal conductivity degradation observed in the subject temperature range [16]. However, these two methods for irradiation temperature estimation involve relatively large error due to the quantitative uncertainty in reference values. Moreover, both the swelling and the thermal conductivity degradation

Table 4
Mass density and swelling of monolithic CVD SiC samples. Numbers in parentheses indicate standard deviations.

Condition	# Samples	Density (g/cm^3)	Swelling (%)
Non-irradiated	3	3.2104 (0)	
850 °C/3.5 dpa	1	3.1944	0.49
450 °C/2.0 dpa	1	3.1700	1.25
440 °C/0.8 dpa	1	3.1685	1.29
860 °C/5.3 dpa	1	3.1941	0.50
500 °C/3.0 dpa	1	3.1766	1.04
790–840 °C/3.4–3.5 dpa	9	3.1936 (0.0028)	0.53 (0.09)

are subject to potentially significant enhancement during the reactor shut-down sequences. On the other hand, annealing analysis often provides a better temperature resolution. In the present case, however, as shown in the plot of ambient temperature reciprocal thermal diffusivity against the annealing/measurement temperature, Fig. 1 an explicit determination of the onset temperature for defect annealing was not always possible for the irradiated CVD SiC. Typically, the onset of defect annealing is most explicitly seen by deviation from the linear relationship between the reciprocal thermal diffusivity and the annealing temperature. Therefore, the nominal irradiation temperature was determined based primarily on an estimate from the thermal diffusivity recovery when it involves an explicit recovery onset, whereas otherwise it was determined based primarily on the densitometry result but was also

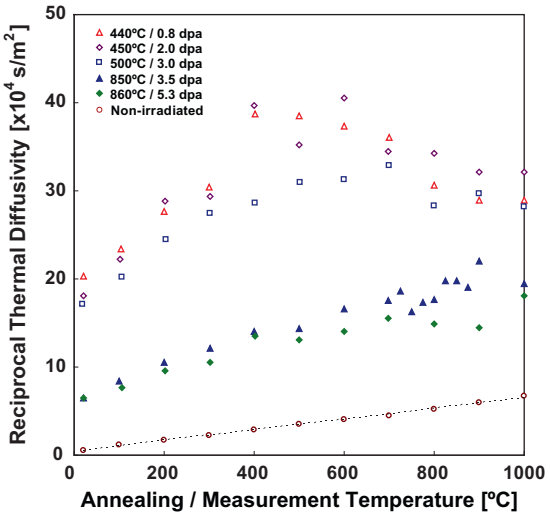

Fig. 1. Annealing behavior of reciprocal thermal diffusivity of irradiated CVD SiC samples. The non-irradiated data points are averages of five pre-irradiation values for the irradiated specimens (standard deviations are smaller than size of the symbols).

Table 3
Estimation of irradiation temperatures for CVD SiC samples.

Capsule ID	Vertical position of temperature monitor in capsule	Design temperature (°C)	Estimate from TD[a] recovery (°C)	Estimate from DGC[b] density (°C)	Estimate from reciprocal thermal conductivity (°C)	Revised nominal irradiation temperature (°C)
SC-03-1	Center	788	950 ± 100	790 ± 100	780 ± 100	850
SC-03-2	Bottom	404	450 ± 25	450 ± 100	470 ± 100	450
SC-03-3	Bottom	410	440 ± 40	440 + 50/−100	440 ± 100	440
SC-03-4	Bottom	977	860 ± 100	800 ± 100	800 ± 100	860
SC-03-5	Bottom	743	760 ± 40	510 ± 50	490 ± 100	500

[a] Thermal diffusivity.
[b] Density gradient column.

Table 5
Thermal conductivity for non-irradiated and irradiated monolithic SiC at 20 °C. Numbers in parentheses indicate standard deviations.

Nominal condition	CVD SiC			SA3 CVI			HNLS CVI	
	Thermal diffusivity (m^2/s)	Thermal conductivity (W/m-K)	Mass density (g/cm^3)	Thermal diffusivity (m^2/s)	Thermal conductivity (W/m-K)	Mass density (g/cm^3)	Thermal diffusivity (m^2/s)	Thermal conductivity (W/m-K)
Non-irradiated	$1.24(0.04) \times 10^{-4}$	255 (7.4)	2.51 (0.04)	$1.36(0.12) \times 10^{-5}$	22.9 (2.2)	2.42 (0.07)	$5.1(0.9) \times 10^{-6}$	8.5 (2.0)
850 °C/3.5 dpa	1.54×10^{-5}	31.9	2.54	3.3×10^{-6}	5.6	2.44	1.5×10^{-6}	2.4
450 °C/2.0 dpa	5.5×10^{-6}	11.4	2.45	2.0×10^{-6}	3.3	2.37	1.0×10^{-6}	1.5
440 °C/0.8 dpa	4.9×10^{-6}	10.2	2.53	2.3×10^{-6}	3.8	2.35	0.9×10^{-6}	1.3
860 °C/5.3 dpa	1.55×10^{-5}	32.0	2.53	4.3×10^{-6}	7.3	2.42	1.6×10^{-6}	2.6
500 °C/3.0 dpa	5.8×10^{-6}	12.0	2.52	2.4×10^{-6}	3.9	2.52	1.4×10^{-6}	2.4

adjusted considering the estimates from two other methods. It is considered that the nominal irradiation temperatures in the present work typically involve errors on the order of 100 K. The results of densitometry and the ambient temperature thermal diffusivity/conductivity measurement are summarized in Table 5.

Dynamic Young's modulus was measured using bend bar specimens of CVD SiC, which were irradiated in a nominal temperature range 640–1080 °C. The measured modulus values were highly reproducible, but the irradiated specimens exhibited increased specimen-to-specimen variations compared to the non-irradiated specimens, as shown in Table 6. Despite the increased specimen-to-specimen variations, the irradiated specimens' Young's moduli could confidently be determined to be reduced by 0.5–5.2% from the non-irradiated values. The magnitude of the irradiation-induced Young's modulus decrease appeared greater for the lower irradiation temperature, Fig. 2.

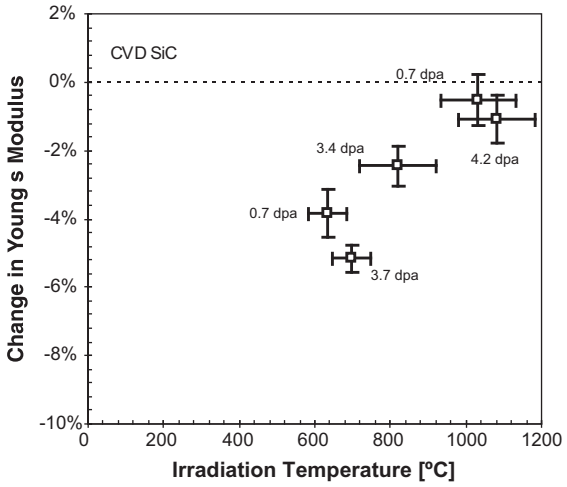

Fig. 2. Changes in ambient temperature Young's modulus for neutron-irradiated CVD SiC as a function of irradiation temperature.

3.2. Composite thermal properties

Thermal diffusivity and conductivity of the irradiated composite samples are summarized in Table 5. The thermal conductivity values were derived using the measured thermal diffusivity, measured apparent mass density, and literature values of heat capacity for beta-phase SiC [2]. The values for the non-irradiated condition are averages of pre-irradiation values for the irradiated specimens. The non-irradiated thermal conductivity for the SA3 composite specimens is typical of the similar materials[17]. On the other hand, that for the HNLS composite specimens is significantly lower than typical [17,18]. The reason for the low thermal conductivity is likely the low mass density, or high porosity, of the particular thermal diffusivity specimens used.

In Fig. 3, reciprocal thermal diffusivities for the irradiated and non-irradiated composite specimens are plotted against annealing/test temperature. The elevated temperature measurement was made after 30 min thermal equilibration at each temperature. Similar to monolithic SiC, reciprocal thermal diffusivity for the irradiated composite specimens exhibits a linear temperature dependence until thermal recovery of the irradiation-produced defects takes place. Compared to the SA3 composite, the HNLS composite exhibited not only a lower ambient temperature thermal diffusivity but also greater temperature coefficients of reciprocal thermal diffusivity in both non-irradiated and irradiated conditions, and a greater effect of neutron irradiation (note the difference in vertical scales in Fig. 3).

Table 6
Young's moduli for non-irradiated and irradiated monolithic SiC as determined by impulse excitation and sonic resonance method. Numbers in parentheses indicate standard deviations.

Nominal irradiation condition	Specimen dimensions (mm)	# Samples	Modulus (GPa)	Modulus change
Non-irradiated	25 × 2 × 1.5	8	448.5 (1.2)	
640 °C/3.7 dpa		2	431.3 (3.1)	−3.8 (0.7)%
700 °C/0.7 dpa		2	425.4 (1.8)	−5.2 (0.4)%
1030 °C/0.7 dpa		2	446.2 (3.3)	−0.5 (0.7)%
1080 °C/4.2 dpa		2	443.7 (3.1)	−1.1 (0.7)%
Non-irradiated	51 × 6.3 × 3.2	5	459.2 (0.8)	
820 °C/3.4 dpa		12	448.0 (2.7)	−2.4 (0.6)%

3.3. Preliminary evaluation of composite tensile behavior

Typical non-irradiated tensile behaviors for the HNLS and the SA3 composites during the cyclic tensile tests are compared in Fig. 4. In the stress–strain envelope curve, the end of the initial linear regime approximately corresponds to the stress and strain at which a major matrix micro-crack developed and started to open, whereas the additional matrix micro-cracks progressively developed during the second linear regime [19]. The second linear regime ends as the matrix micro-crack density saturates, when the load is carried only by the bridging fibers, thus the progressive fail-

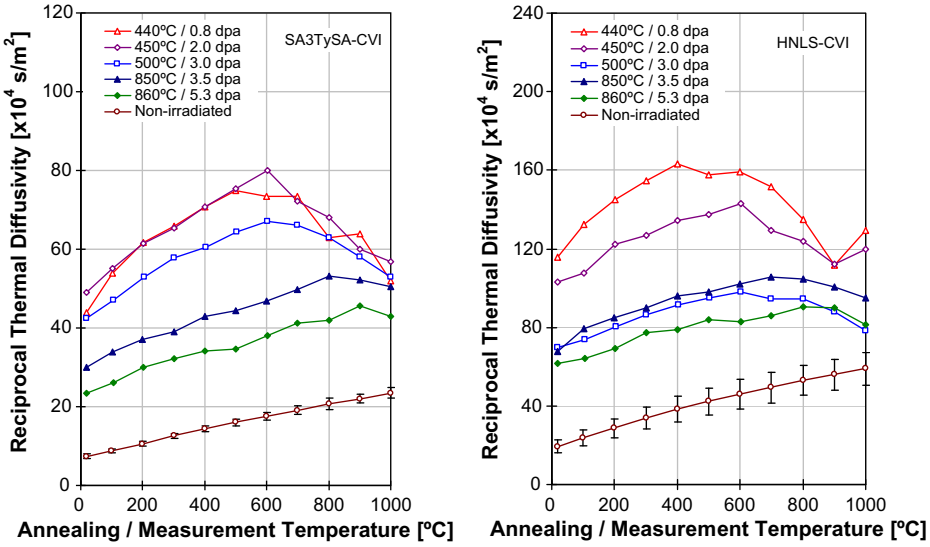

Fig. 3. Annealing behavior of reciprocal thermal diffusivity of irradiated CVI SiC/SiC samples. The non-irradiated data points are averages of five pre-irradiation values for the irradiated specimens (Error bars indicate one standard deviation).

ure of the fibers causes a gradual decrease in the composite modulus. The examples in Fig. 4 indicate that the HNLS and the SA3 composites failed after and likely before the matrix crack saturation, respectively. Such behaviors are typical for the respective composites [20,21].

As the preliminary evaluation of the composite tensile behavior, specimens of the HNLS composites were tested in monotonic and cyclic loading modes. Fifteen randomly selected specimens were tested in each mode, and the results are summarized in Table 7 along with the results for the irradiated specimens. The results confirmed the very good reproducibility of all the properties measured, including tensile modulus, proportional limit stress and strain, ultimate tensile stress, and strain at load maximum. Moreover, differences in those properties between the monotonic and cyclic loading mode were not observed. The Weibull statistical parameters in the monotonic and cyclic modes are compared in Fig. 5, in which the maximum likelihood estimations in one testing mode are within the 95% confidence ratio ring in the other testing mode, indicating no statistically significant difference. It is noteworthy that a Weibull modulus of ~16 is obtained for the UTS in both test modes combined. This also proves validity of the miniature specimen test geometry and procedure adopted for the purpose of present research.

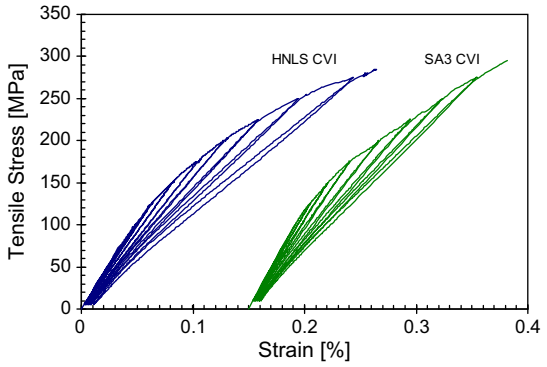

Fig. 4. Typical tensile stress–strain behaviors of Hi-Nicalon™ Type-S and Tyrano™-SA3 composites.

3.4. Neutron irradiation effects on composite tensile properties

The irradiated tensile properties are summarized in Table 7. Also, in Fig. 6, the PLS and the UTS are plotted against neutron dose regardless of irradiation temperature. The only apparent significant effect of irradiation is the decrease in UTS of the HNLS composites at doses of <~3 dpa. In fact, the tensile modulus and the PLS of both the composites and the UTS of the SA3 composite remained unchanged considering the statistical uncertainty. The UTS of the HNLS composites at ~1000 °C and 5.3 dpa, where statistically significant number of specimens were irradiated and tested, appeared comparable with the non-irradiated value. These results confirm the general insensitivity of both types of the composites to neutron irradiation.

In Figs. 7 and 8, the stress–strain curves involving the cyclic unloading/reloading sequences are compared for the HNLS and SA3 composites, respectively, before and after irradiation to the highest doses. Both sets of data show that no significant change in the envelope curve took place in either composite. It is noted that the width of the hysteresis loops generally enlarged after irradiation for the HNLS composites irradiated to ~5.3 dpa at ~1000 °C, whereas such a change is not apparent for the SA3 composites irradiated to ~3.5 dpa at ~780 °C.

There were several irradiated specimens of both types of composites which exhibited anomalous tensile behaviors. Typical stress–strain curves for such cases are presented in Fig. 9. The HNLS composite specimens which exhibited anomalously low UTS typically failed before matrix micro-crack saturation is achieved, unlike the typical failure for this material shown in Fig. 7. The specimens in Fig. 9 are with undamaged matrices, because the initial tensile moduli and the PLSs are normal. Therefore, the possible reasons for the anomalous composite behavior are weak fibers and/or excessively strong interfaces. Meanwhile, the anomalous tensile properties for the SA3 composites specimens typically accompanied both the initial tensile modulus and the PLS significantly being lower than other specimens. These indicate that the matrix micro-cracks had already developed significantly before the testing. Such defects may have been introduced during specimen handling.

In Fig. 10, scanning electron microscopic images are provided for fracture surfaces of the composites in non-irradiated and three

Table 7
Tensile properties for non-irradiated and irradiated SiC composites.

Material	Condition	Loading mode	# of Valid test	Tensile modulus (GPa)	Proportional limit stress (MPa)	Ultimate tensile stress (MPa)	Strain at proportional limit (%)	Strain at load maximum (%)
HNLS CVI	Non-irr. (1)	Monotonic	15	230 (23)	94 (18)	281 (24)	0.04 (0.01)	0.28 (0.07)
	Non-irr. (2)	Cyclic	15	232 (25)	97 (24)	284 (19)	0.04 (0.01)	0.27 (0.05)
	Non-irr. (3)	Cyclic	10	226 (27)	126 (12)	224 (33)	0.06 (0.01)	0.15 (0.04)
	1000 °C/ 5.3 dpa	Cyclic	20	243 (37)	136 (25)	243 (41)	0.06 (0.01)	0.17 (0.06)
	220 °C/ 0.48 dpa	Cyclic	4	204 (24)	121 (17)	251 (21)	0.06 (0.01)	0.20 (0.03)
	350 °C/ 0.97 dpa	Cyclic	4	220 (50)	110 (13)	207 (42)	0.05 (0.01)	0.14 (0.03)
	480 °C/ 1.6 dpa	Cyclic	4	207 (6)	117 (26)	189 (30)	0.06 (0.01)	0.13 (0.04)
	570 °C/ 2.2 dpa	Cyclic	4	197 (19)	116 (12)	171 (38)	0.06 (0.01)	0.11 (0.05)
	610 °C/ 2.8 dpa	Cyclic	3	244 (36)	104 (11)	188 (23)	0.04 (0.01)	0.12 (0.01)
SA3 CVI	Non-irr.	Cyclic	10	218 (32)	112 (30)	266 (33)	0.06 (0.02)	0.22 (0.05)
	380 °C/ 0.31 dpa	Cyclic	4	196 (46)	75[a] (42)	218[a] (40)	0.04[a] (0.01)	0.21[a] (0.04)
	400 °C/ 0.62 dpa	Cyclic	2	219 (16)	128 (2)	261 (16)	0.06 (0)	0.23 (0.02)
	420 °C/ 1.0 dpa	Cyclic	3	251 (40)	131 (23)	259 (37)	0.05 (0.01)	0.18 (0.06)
	460 °C/ 1.4 dpa	Cyclic	4	209 (21)	104 (13)	275 (30)	0.05 (0.01)	0.24 (0.06)
	480 °C/ 1.8 dpa	Cyclic	4	203 (21)	81[a] (18)	267 (17)	0.04[a] (0.01)	0.26 (0.03)
	780 °C/ 3.5 dpa	Cyclic	4	220 (9)	104 (12)	266 (29)	0.05 (0.01)	0.27 (0.05)
	760 °C/ 3.0 dpa	Cyclic	4	208 (6)	83[a] (19)	248 (17)	0.04[a] (0.01)	0.26 (0.04)
	690 °C/ 2.5 dpa	Cyclic	3	188[a] (42)	74[a] (4)	237 (31)	0.04[a] (0.01)	0.25 (0.05)
	610 °C/ 1.9 dpa	Cyclic	4	205 (14)	89 (14)	243 (36)	0.05 (0.01)	0.25 (0.07)
	530 °C/ 1.2 dpa	Cyclic	3	219 (14)	81 (17)	264 (15)	0.04 (0.01)	0.26 (0.03)

[a] Average and standard deviations are affected by anomalous data points due likely to defective specimens.

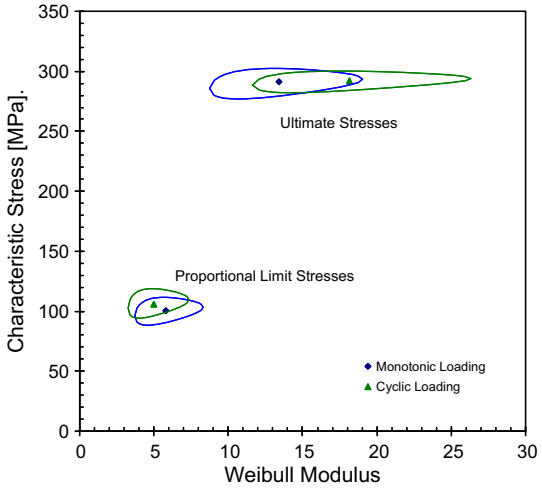

Fig. 5. Statistical parameters for tensile proportional limit and ultimate stresses for Hi-Nicalon™ Type-S composite tested in monotonic and cyclic loading modes. The symbols and the rings represent the maximum likelihood estimation and the 95% confidence ratio bounds, respectively.

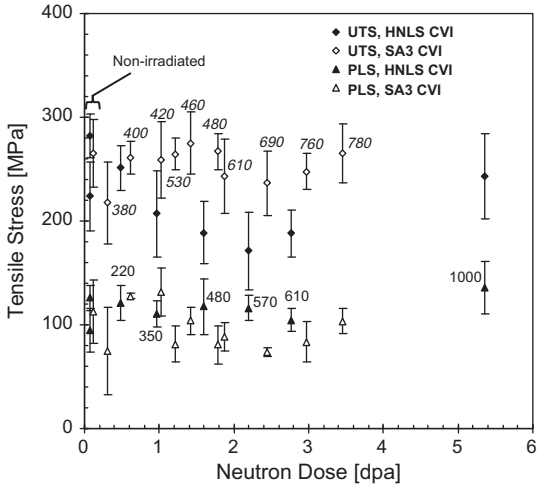

Fig. 6. Effect of neutron dose on tensile proportional limit and ultimate tensile stresses for composites. Data labels indicate the nominal irradiation temperature in °C for Hi-Nicalon Type-S (upright) and Tyranno-SA3 (oblique) composites.

different irradiation conditions. The fracture surfaces shown in the low magnification micrographs are rather brittle, showing that the interfacial frictional stresses in these composites are relatively high. While the typical fiber pull-out length was 5–10 μm in the non-irradiation condition, it became slightly longer (5–20 μm) after irradiation at ~570 °C–2.2 dpa or at ~1000 °C–5.3 dpa. Con-

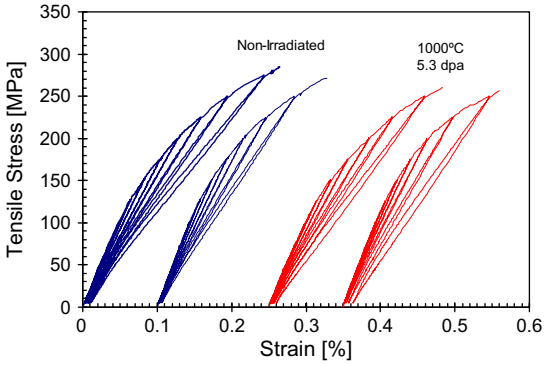

Fig. 7. Comparison of tensile stress–strain behaviors for non-irradiated and irradiated Hi-Nicalon™ Type-S composites.

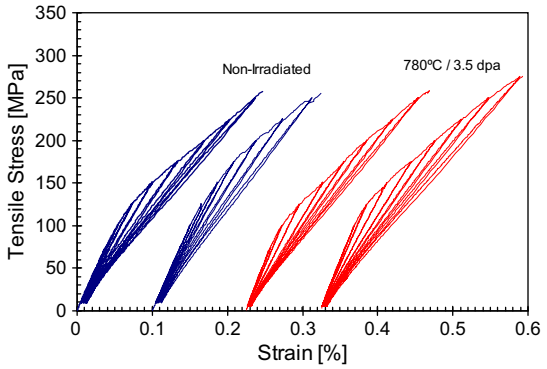

Fig. 8. Comparison of tensile stress–strain behaviors for non-irradiated and irradiated Tyranno™-SA3 composites.

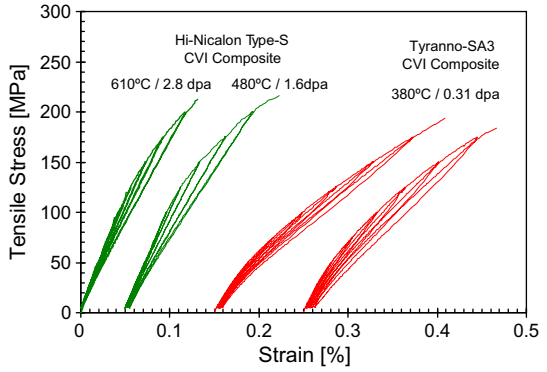

Fig. 9. Examples of stress–strain behaviors for irradiated specimens which exhibited poor tensile properties.

trarily, fracture surface of the composite irradiated at ~350 °C–1 dpa appeared more brittle with the typical fiber pull-out length <5 μm. There was no noticeable effect of irradiation on fracture surface appearance of the SA3 composites, showing the typical fiber pull-out length 5–30 μm in all conditions.

3.5. Fiber strength

Result of the single fiber tensile strength measurement is summarized in Table 8. 30–40 fiber specimens were tested for each condition for the purpose of statistical analysis. The non-irradiated SA3 and HNLS fibers exhibited the Weibull mean strength of 1.85 GPa and 2.32 GPa, respectively. Neutron irradiation at below ~770 °C caused increases in characteristic strength for both types of fibers. Meanwhile, both fibers irradiated to 5.3 dpa at ~910 °C underwent significant reduction in characteristic strength. Weibull moduli generally increased or remained unchanged after irradiation.

Fig. 11 shows the dose dependence of Weibull mean strength for neutron-irradiated SA3 and HNLS fibers. Data on HNLS fibers by Nozawa et al. in a previous experiment are plotted together [22]. These results indicate that neutron irradiation at <~800 °C does not cause strength degradation, but rather minor strengthening, of either type SiC fiber. Neutron irradiation of bare fibers at higher temperatures apparently caused significant strength degradation. However, examination by scanning electron microscopy did not reveal the influence of irradiation on the surface appearance of the fibers, Fig. 12.

4. Discussion

4.1. Thermal conductivity decrease

Irradiation-induced thermal conductivity degradation in crystalline SiC has been studied for decades and now it is well known that: (1) a rapid change in thermal conductivity takes place as soon as irradiation starts and it tends to saturate before a few dpa is reached at irradiation temperatures above the amorphization threshold and below ~1000 °C, (2) the magnitude of the saturated swelling is greater at lower irradiation temperatures, and (3) the observed thermal conductivity decrease is caused by accumulation of lattice point defects and clusters of various types [2]. All the vacancies, self interstitial atoms, antisite defects, and their clusters are believed to contribute to the thermal conductivity decrease. Quantitative contributions from different defect species to thermal conductivity decrease have not sufficiently been studied [23,24]. Recently, Snead et al. found that the magnitude of swelling is linearly correlated with "defect thermal resistance," $1/K_{rd}$, regardless of irradiation condition within the saturable swelling temperature regime [16]. The defect thermal resistance is defined as the difference in reciprocal thermal conductivity before and after irradiation, $1/K_{unirr}$ and $1/K_{irrad}$, respectively. This finding implies that the total phonon scattering by various irradiation-produced defects is approximately proportional to the total defect volume.

In Fig. 13, defect thermal resistances of neutron-irradiated CVD SiC are calculated and plotted against isochronal annealing/measurement temperature. The relationship between the defect thermal resistance and swelling obtained here agrees very well with the previously published correlation [16]. The defect thermal resistance in CVD SiC remains nearly constant but slightly increases as the test temperature increases, until defect annealing initiates at above the irradiation temperature. Vacancies and antisites defects are believed to be present at very high concentrations in irradiated SiC, because both are produced at high rates and their mobility is extremely limited in the temperature range of this study [25,26]. Therefore, it is reasonable to assume these two types of defects are primarily responsible for the thermal conductivity decrease. Molecular dynamics simulations by Bus et al. indicates that isolated vacancies impose thermal resistances which decreases with increasing temperature, while the temperature dependence of other defects vary depending on the type and configuration [24]. If this is the case, the temperature dependence of defect thermal resistance observed here indicates that various defect species are

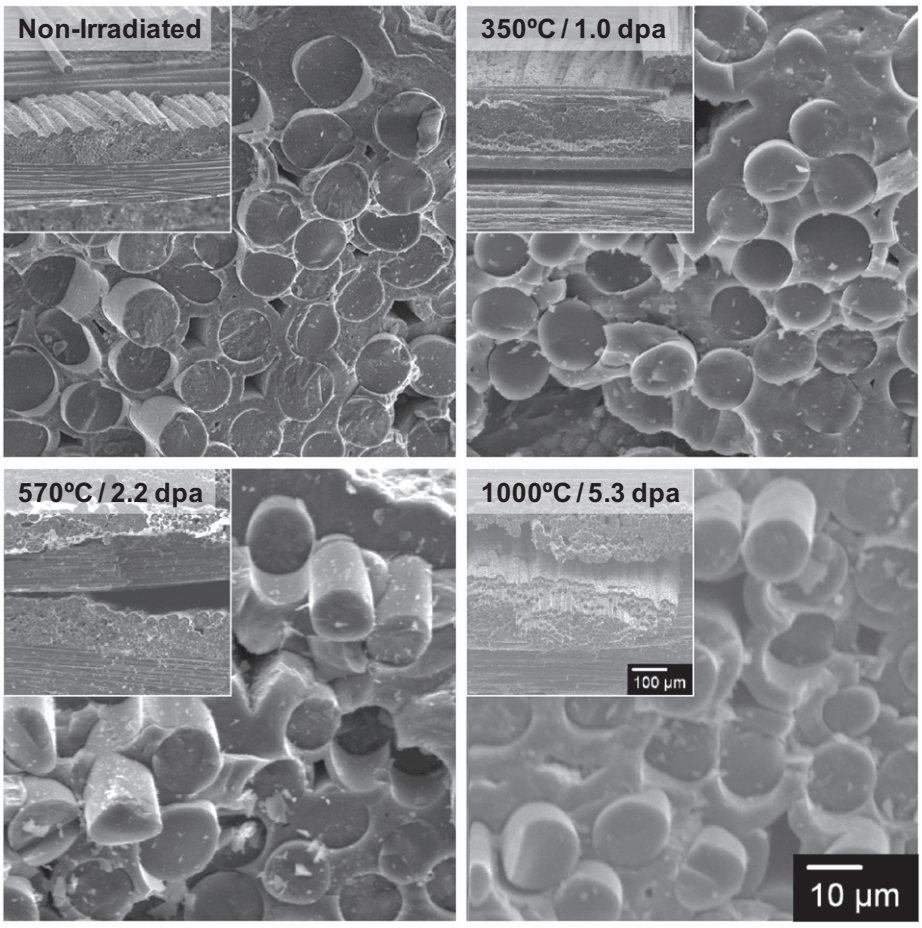

Fig. 10. Secondary scanning electron images of fracture surfaces of Hi-Nicalon™ Type-S CVI composites in non-irradiation and various irradiation conditions.

Table 8
Tensile strength for non-irradiated and irradiated SiC fibers. Numbers in parentheses indicate standard deviations.

Material	Condition	# of Valid test	Fiber diameter (μm)	Weibull modulus	Characteristic strength (GPa)	Mean strength (GPa)	Coefficient of variance
SA3	Non-irr.	38	7.5 (1.1)	3.9	2.03	1.85	0.28
	470 °C/ 1.6 dpa	33	7.4 (0.9)	4.7	2.20	2.04	0.24
	770 °C/ 3.3 dpa	35	7.3 (0.9)	4.8	2.29	2.12	0.24
	910 °C/ 5.3 dpa	40	7.3 (1.0)	3.8	1.74	1.58	0.29
	280 °C/ 0.6 dpa	34	7.1 (1.1)	5.5	2.50	2.34	0.21
HNLS	Non-irr.	39	13.3 (2.6)	2.8	2.64	2.32	0.38
	470 °C/ 1.6 dpa	35	13.5 (1.9)	4.1	2.81	2.57	0.28
	910 °C/ 5.3 dpa	39	13.7 (1.7)	3.9	1.41	1.29	0.29
	280 °C/ 0.6 dpa	39	12.9 (1.4)	3.9	3.20	2.91	0.29

competing rather than only vacancies are governing the irradiated thermal conductivity of CVD SiC.

Defect thermal resistances of CVI composites with two types of SiC fibers are compared in Fig. 14. For the SA3 composite it remained almost constant or very slightly decreased as the annealing/measurement temperature increased, whereas HNLS composite thermal resistance decreased more significantly with temperature. It may be assumed that the defect resistances in CVD SiC and the SA3 composite are roughly constant from ambient to the irradiation temperature, whereas that is not the case for the HNLS composite. The observation implies that the contributions from various defects to the thermal conductivity degradation are different between the SA3 and the HNLS composites due to the differences in impurities and as-fabricated microstructures.

Fig. 15 plots the ambient temperature defect thermal resistance for three materials as a function of irradiation temperature. The defect resistances for the SA3 composite are approximately three times greater than those for CVD SiC in all irradiation conditions.

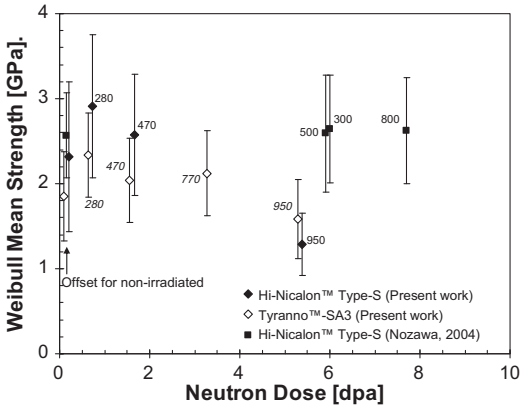

Fig. 11. Effect of neutron irradiation on fiber strength. Data labels indicate the nominal irradiation temperature for Hi-Nicalon Type-S (upright) and Tyranno-SA3 (oblique) fibers.

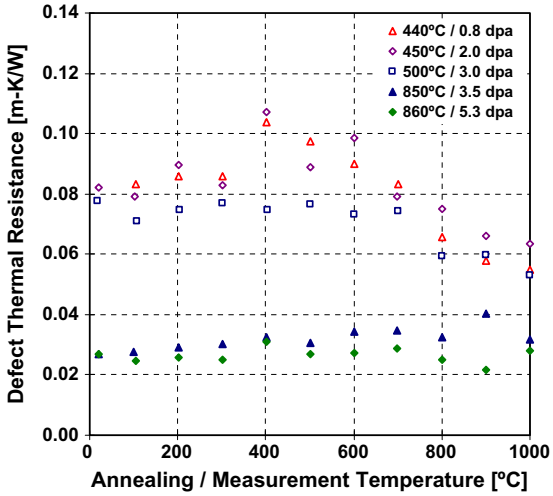

Fig. 13. Temperature dependence of defect thermal resistance for irradiated CVD SiC.

Similarly, the defect thermal resistances for the HNLS composite are approximately twice that of the SA3 composites. Both composite materials have similar fiber volume fractions 30–35% and the other constituents are nominally identical. Therefore, the net difference in defect thermal resistance between the two types of fibers must be substantially more significant than the apparent difference averaged over the composite bodies. Because the main differences between the CVD SiC and SA3 fiber and between the two fibers are in impurity species and amount (Table 1), the reason for such major differences in defect thermal resistance is likely related with the interactions of the residual impurities with irradiation-produced defects. Moreover, as-fabricated microstructures may be the additional factor affecting the defect thermal resistance, because the microstructures such as the sizes and morphologies of the SiC grains, the appearances of the graphite pockets, and the as-grown stacking fault density are very significantly different in these materials (CVD SiC and both fibers). Snead et al. report systematic differences in dose-dependent accumulation and annealing behaviors of defect thermal resistances among CVD SiC, reaction-bonded SiC (both in beta-phase), and alpha-phase SiC sintered with boron [27]. However, the differences observed in this work between CVD SiC and composites are more significant than

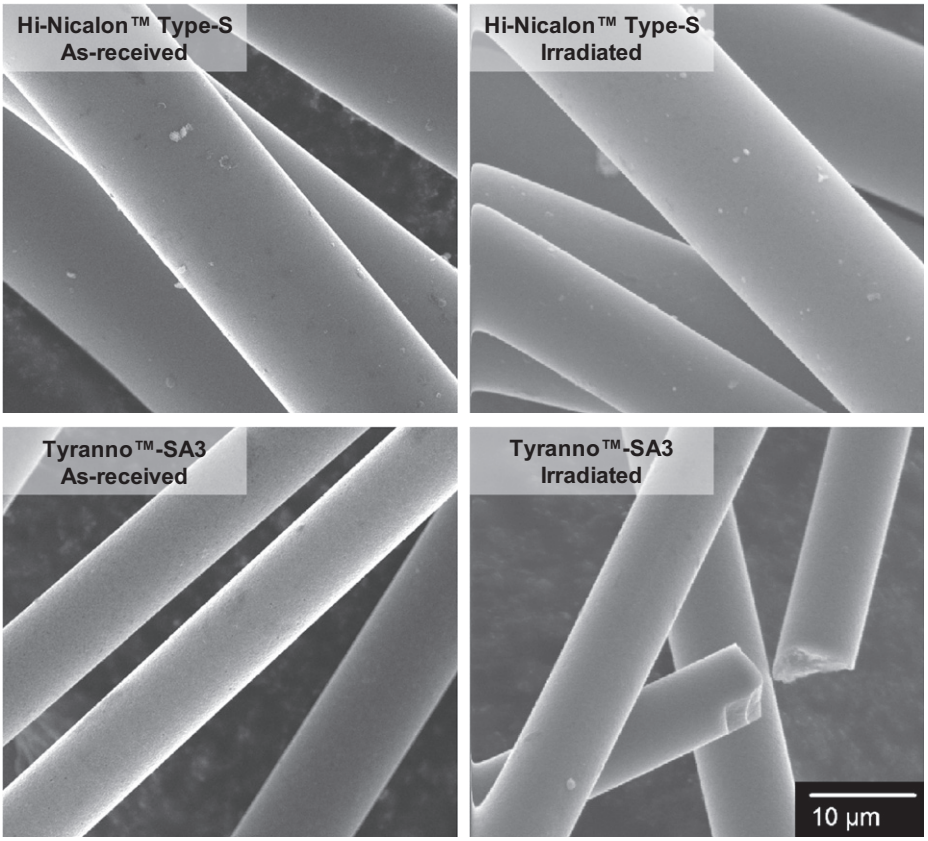

Fig. 12. Secondary electron images of Hi-Nicalon Type-S and Tyranno-SA3 fibers in as-received and irradiated (910 °C, 5.3 dpa) conditions.

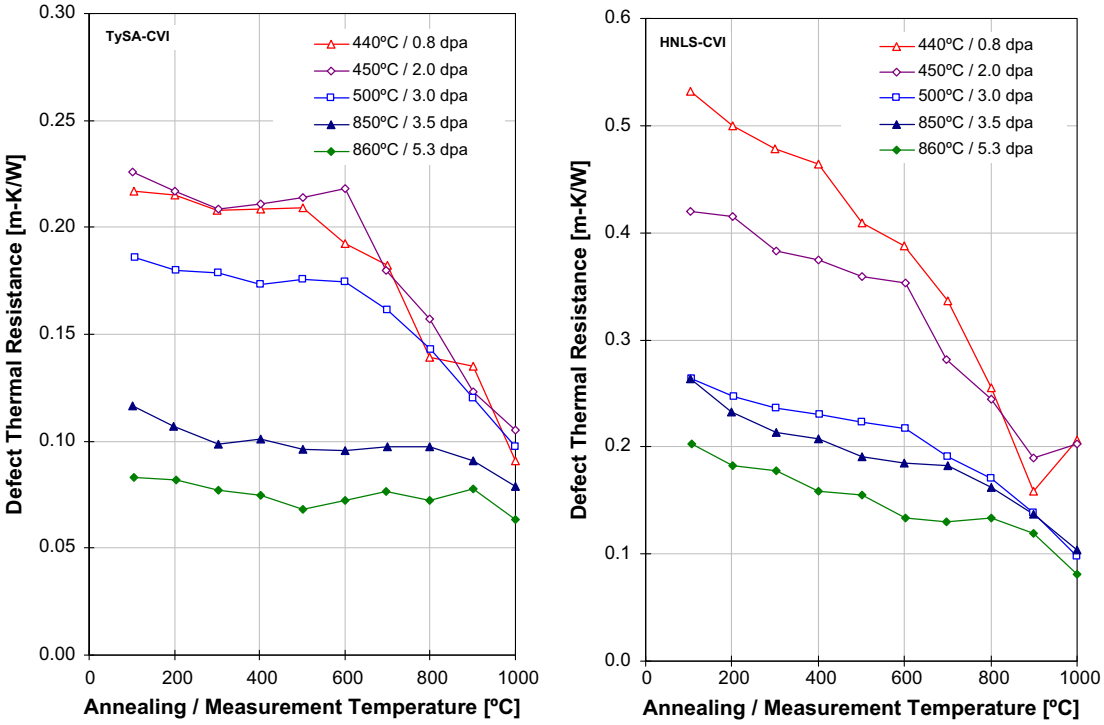

Fig. 14. Temperature dependence of defect thermal resistance for irradiated composites.

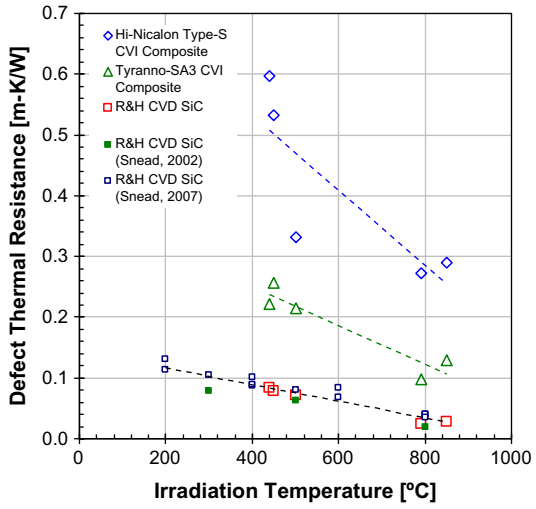

Fig. 15. Ambient temperature defect thermal resistance for irradiated CVD SiC and CVI composites as a function of irradiation temperature.

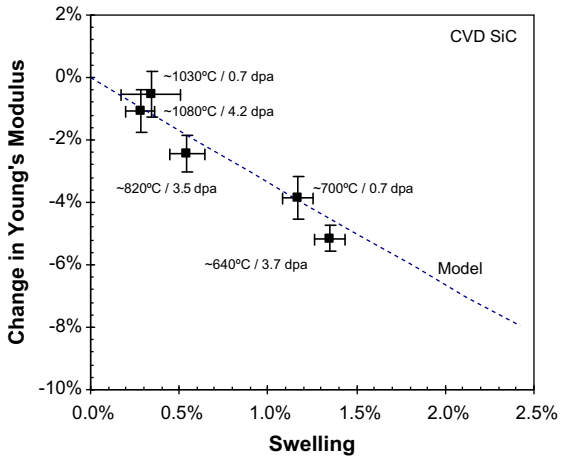

Fig. 16. Correlation between volumetric swelling and change in Young's modulus for neutron-irradiated CVD SiC. Dashed line indicates prediction of modulus decrease by uniform lattice swelling based Tersoff model.

those reported between CVD SiC and other impure monolithic SiC. Therefore, the defect accumulation/recovery behaviors in CVD SiC, SA3, and HNLS during irradiation will be significantly different.

4.2. Mechanical properties

Young's moduli of the CVD SiC specimens at ambient temperature decreased by 0.5–5.2% from the non-irradiated values depending on irradiation conditions. Because detectable Young's moduli decreases occur in irradiated SiC within the temperature range where saturable swelling accompanies lattice expansion, Katoh et al. correlated the modulus change with swelling of SiC [28]. Saturable swelling, which occurs in crystalline SiC above amorphization threshold temperature and below ~1000 °C, is believed to be caused by accumulation of point defects and tiny defect clusters, and is accompanied by lattice expansion measured by X-ray diffraction to almost exactly correspond to the magnitude of macroscopic linear swelling [26,29]. In Fig. 16, the changes in Young's modulus are plotted against the magnitude of swelling. The dashed line in Fig. 16 indicates the prediction of modulus decrease by a uniform lattice swelling based on Tersoff's model of interatomic force in SiC [30]. The approximately linear correlation between modulus change and swelling is obvious in the irradiation temperature range in this study, and the modulus changes appear quantitatively consistent with the prediction by Tersoff model. This observation indicates correlations among elastic modulus change,

swelling, and thermal conductivity decrease for SiC irradiated in the temperature regime for saturable swelling.

Evaluation of the irradiation-induced tensile moduli changes for composites is less useful than Young's modulus for CVD SiC because of the very significant data scatter. The average tensile moduli for the HNLS composites in non-irradiated, ~1000 °C-irradiated, and (220–610)°C-irradiated conditions were 232, 243, and 213 GPa, respectively. Considering the typical standard deviations of 25–40 GPa, the apparent slight modulus increase at ~1000 °C is statistically insignificant, whereas the decrease at <610 °C may be significant. Assuming that the composites' tensile modulus change is dictated by the Young's modulus change in the matrix SiC, one may expect <1% and >5% modulus decrease at ~1000 °C and <610 °C, respectively. As for the SA3 composites, the non-irradiated average tensile modulus 218 GPa decreased to 211 GPa after irradiation at 380–780 °C. This change is statistically insignificant but consistent with the anticipated Young's modulus decrease (~5%) in the matrix. It should be noted that the irradiation-induced Young's moduli changes in CVD SiC, SA3 and HNLS may be significantly different, because a significant difference in defect thermal resistance was observed.

Tensile PLS of both the HNLS and SA3 composites remain unchanged within the statistical uncertainty after irradiation. The PLS is typically interpreted as the stress at which a micro-crack propagates across the specimen in a transverse direction [19]. The micro-cracking in two-dimensional woven fabric composites during tensile loading in 0°/90° orientation is generally considered to originate at interphases within the transverse (90°) fiber bundle and propagate into the matrix, to initiate at the pore surface where the intense stress concentration occurs, or to be pre-existing [31,32]. The PLS is determined mainly by shape and size of the crack-initiating bundle or pore, thermal residual stress in and fracture energy of the matrix, and the frictional stress at the fiber–matrix interface [19,33]. Ignoring the interfacial bonding effect and the Poisson effect, a simple formulation of the stress for transverse matrix cracking in uni-directional fiber composites is given by:

$$\sigma_{mc} = \left[\frac{6\tau\gamma_m}{r}\cdot\frac{f^2E_fE_c^2}{(1-f)E_m^2}\right]^{1/3} - \sigma_T \tag{1}$$

using interfacial frictional stress (τ), matrix fracture energy (γ_m), fiber radius (r), volume fraction of axial fibers (f), Young's modulus of fiber, matrix, or composite ($E_{f,m,c}$), and residual stress (σ_T) [34]. Neutron irradiation may cause significant modifications in the interfacial frictional stress and residual stress. Although the matrix fracture energy and the constituents' moduli may slightly change, their impact would be minimal because of the one-third exponent in Eq. (1). For the same reason, significant modification in the interfacial frictional stress results in only minor modification to the PLS. Based on the regression line analysis [35], the axial residual stresses were estimated to be 20–40 MPa compressive in the matrices, regardless of non-irradiated or irradiated conditions for composites with both fiber types. Observed lack of a significant PLS change is thus considered reasonable. The fiber–matrix interfacial frictional stress is an important parameter that strongly influences the fracture behavior of continuous fiber composites. Here the irradiation effect on the interfacial frictional stress is further examined by analyzing the unloading–reloading hysteresis. The width of the hysteresis loop at the half peak stress ($\delta\varepsilon_{1/2}$) can be related with the interfacial sliding stress (τ) and the mean matrix crack spacing ($\bar{d}$) by the following equation [19]:

$$\delta\varepsilon_{1/2} = \frac{b_2(1-a_1V_f)^2\sigma_p^2}{8f^2\tau E_m}\cdot\frac{r}{\bar{d}} \tag{2}$$

with peak stress before unloading (σ_p), and Hutchinson–Jensen parameters (a_1, b_2) [36]. The matrix crack spacing is ideally inversely proportional to the matrix damage parameter (D) as defined in the following equation [37]:

$$D = \frac{E_c - E^*}{E^*} \tag{3}$$

where E^* is the tangent modulus of the unloading curve. Using the relationship of D with $\bar{d}$, Eq. (2) is rewritten as:

$$\delta\varepsilon_{1/2} = K\cdot\frac{D\sigma_p^2}{\tau} \tag{4}$$

using a constant K which is only very slightly affected by irradiation.

In Fig. 17, the loop width $\delta\varepsilon_{1/2}$ is plotted against $D\sigma_p^2$ for both composites in non-irradiated and irradiated conditions. Although the data scatter is significant for all conditions, it is rather obvious that interfacial frictional stress in the HNLS composite decreased to approximately 2/3 of the non-irradiated value after irradiation to 5.3 dpa at ~1000 °C. Effect of irradiation at lower temperatures on interfacial properties of the HNLS composite could not be analyzed in this way due to the insufficient extent of the second linear

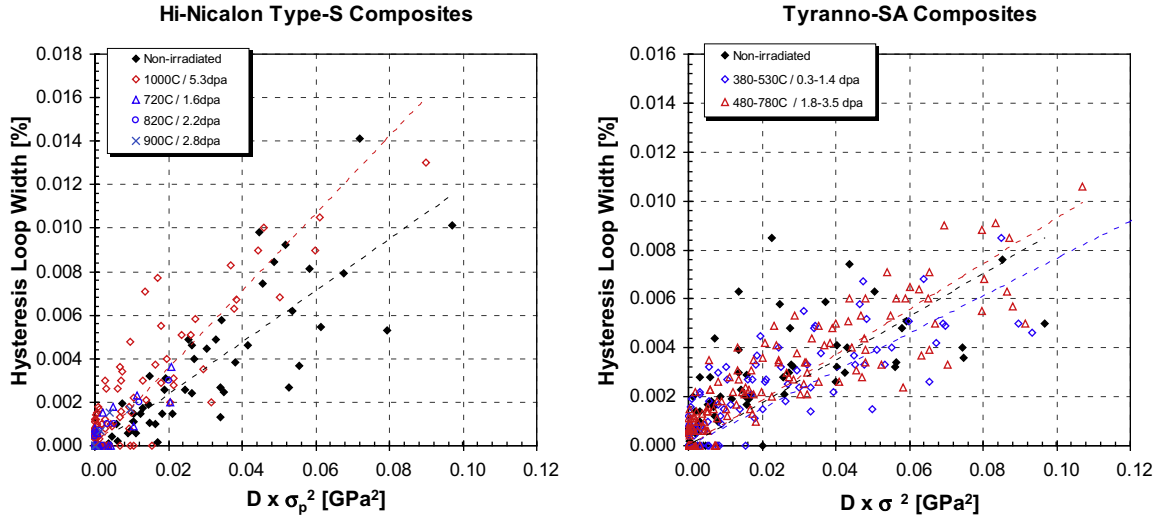

Fig. 17. Comparison of hysteresis loop width vs. matrix damage parameter before and after irradiation for Hi-Nicalon™ Type-S and Tyranno™-SA3 composites.

deformation. On the contrary, the SA3 composite maintained the non-irradiated interfacial frictional stress after irradiation.

The interfacial frictional stress may also be estimated from the fiber pull-out length, since the pull-out length is inversely proportional to the frictional stress under constant fiber strength properties [38]. The extent of frictional stress decrease estimated above for the HNLS composites irradiated at ~1000 °C is consistent with the slight pull-out length increase observed by fractography.

There are two likely explanations for the observed difference between the two composites in irradiation effect on the frictional stress: (1) a difference in irradiation conditions and (2) the effect of physical roughness of the interface. Interfacial debonding in the (PyC/SiC) multilayered interphase composites occurs mostly at the innermost PyC layer [39]. PyC is known to degrade its mechanical properties under intense neutron irradiation, and the degradation occurs earlier at a higher temperature [40,41]. The high irradiation temperature for the HNLS composite may have caused the reduction in shear strength of the PyC layer at a relatively low dose. Also, the surface of the HNLS fibers is substantially smoother than that of the SA3 fibers. Hence, due to a mechanical interlocking effect, potential strength degradation in the interfacial layer may not immediately lead to frictional stress reduction in the SA3 composite.

The UTS of continuous fiber composites in an orientation parallel to one of fiber directions is governed by the fiber mechanical properties unless the fiber–matrix interfacial bonding and/or friction are excessively strong. When debonded bridging fibers are solely carrying the load, the maximum apparent stress in composite is analytically described by

$$\sigma_u = f\sigma_0^{m/(m+1)}\left(\frac{\tau L_0}{r}\cdot\frac{2}{m+2}\right)^{1/(m+1)}\frac{m+1}{m+2} \quad (5)$$

with Weibull scale parameters for fiber strength and length (σ_0, L_0), and Weibull modulus for fiber strength (m) [34]. Thus, the statistical strength properties of fibers are the most important factors which determine the composite UTS.

In Figs. 18 and 19, effects of neutron irradiation on statistical tensile strength properties of HNLS and SA3 fibers are presented. The rings around the data points indicate 95% confidence bounds. Additional data for HNLS imported from the previously published HFIR-14 J experiment are plotted [22]. The Weibull moduli for strength of non-irradiated HNLS are inconsistent between two experiments for unknown reasons. However, the irradiated Weibull moduli consistently fall in a range 3–5 regardless of the non-irradiated values. The strength degradation due to irradiation at ~910 °C–5.3 dpa is statistically very significant. In other irradiation conditions, i.e. at <800 °C, strength changes did not appear to be very significant. As for the SA3 fibers, the irradiation-induced changes in Weibull moduli and Weibull characteristic strength were both insignificant, except that a slight yet significant strengthening was observed after irradiation at ~280 °C–0.6 dpa. Moreover, fiber strength after irradiation at ~910 °C–5.3 dpa was significantly lower than after irradiation at lower temperatures, although the change from the non-irradiated strength appeared minor. Weibull moduli for the strength of non-irradiated and irradiated SA3 fibers were consistently in a range 3–5.

With the typical Weibull modulus values of ~4 as a constant, Eq. (5) indicates that the UTS is determined by the fiber strength almost as a single major factor unless a very major variation in the interfacial frictional stress is anticipated. Therefore, the lack of composite UTS decrease after irradiation implies a lack of fiber strength degradation. This means that, although the strength of the HNLS fiber underwent a major degradation when irradiated as bare fibers at ~910 °C–5.3 dpa, strength of the identical fibers was maintained when irradiated in a form of CVI SiC-matrix composite at ~1000 °C–5.3 dpa. In other words, evolution of SiC fiber strength during high temperatures irradiation may be substantially different for bare fiber irradiation and for composite irradiation. The fiber irradiation was carried out in a hermetic capsule filled with inert gas. As stated before, scanning electron microscopy examination did not reveal changes in morphology of the fiber surface. The reason for the strength degradation during the bare fiber irradiation remains undetermined.

The interesting result from the present composite tensile strength evaluation is that the UTS of HNLS composite apparently decreased after irradiation to low doses at relatively low temperatures (<~600 °C/<3 dpa), whereas such a decrease did not occur after irradiation to a higher dose at higher temperature (~1000 °C/5.3 dpa). At ~1000 °C/5.3 dpa, fibers in the composite specimens likely maintained the pre-irradiation strength, and the moderate reduction in the interfacial frictional stress did not significantly affect the composite's mechanical properties. On the other hand, at <~600 °C/<3 dpa, the fiber strength was maintained but the hysteresis analysis failed to provide estimation of the interfacial frictional stress. However, given the reduced fiber pull-out length, excessive frictional stress could have caused the deterioration of composite strength, if the significant UTS reduction is real.

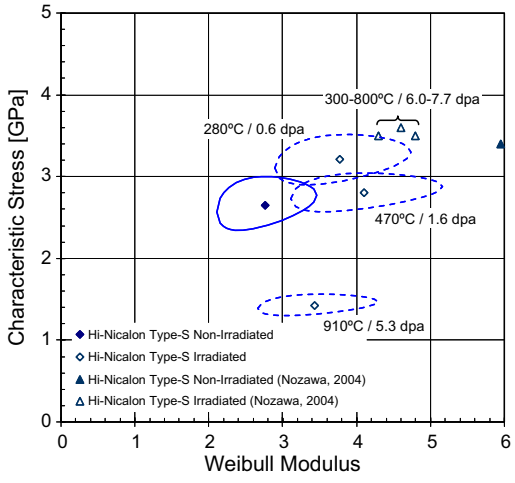

Fig. 18. Statistical tensile strength for Hi-Nicalon™ Type-S fibers.

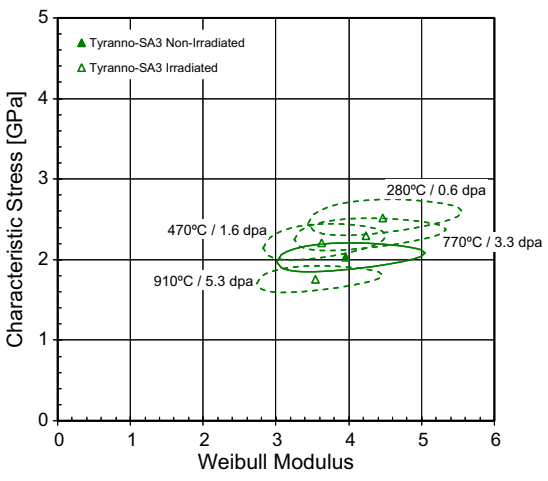

Fig. 19. Statistical tensile strength for Tyranno™-SA3 fibers.

Through the thermal properties analysis, significantly higher defect thermal resistance in the HNLS fiber was found in comparison to those in SA3 and CVD SiC. One explanation for the higher defect thermal resistance is the reduced availability of freely migrating self interstitial atoms which annihilate with the vacancy defects, thus possibly enhance swelling at low to intermediate temperatures. Therefore, it is possible that HNLS fibers undergo greater swelling than the CVI SiC matrices to enhance the interfacial friction in a certain temperature/dose range. A small difference in swelling can cause very significant clamping stresses given the high elastic modulus of SiC. This may also be the case for SA3 composites, though to a more limited extent, because the defect thermal resistance in SA3 is significantly greater than that in the matrices. However, in irradiation conditions studied in the present work, the SA3 fiber or composite did not exhibit significant changes in either of the composite UTS, fiber strength, or interfacial frictional stress.

5. Conclusions

Thermophysical and mechanical properties of CVD SiC and CVI SiC matrix, PyC/SiC multilayered interphase composites with HNLS and SA3 SiC fibers were evaluated following neutron irradiation.

Thermal diffusivity/conductivity of all materials decreased during irradiation, depending primarily on the irradiation temperature. The reciprocal thermal diffusivity linearly increased with temperature from ambient to the anticipated irradiation temperature. Dependency of the defect thermal resistance on annealing/measurement temperature was almost constant (or slightly positive) for the CVD SiC, slightly negative for the SA3 composite, and more significantly negative for the HNLS composite. The magnitude of the defect thermal resistance was distinctively different among materials and its ranking was HNLS > SA3 > CVD SiC regardless of irradiation condition. These observations imply significant difference in defect accumulation/dynamic recovery behaviors among materials, due likely to an impurity effect, since each material had different impurity levels.

Preliminary evaluation of non-irradiated tensile properties of the HNLS composite did not reveal significant difference between the monotonic and the cyclic loading modes in any of the modulus, the PLS, or the UTS. Weibull modulus of $\sim$16 was obtained for the UTS, supporting the adequacy of the miniature specimen geometry and the test procedure adopted.

Dynamic Young's moduli of the irradiated CVD SiC slightly decreased by irradiation. Extent of the modulus decrease appeared clearly correlated with swelling. The modulus–swelling correlation was consistent with the prediction based on an empirical interatomic potential for cubic SiC assuming uniform lattice swelling. This finding implies the ternary correlation among elastic modulus, swelling, and defect thermal resistance in SiC.

No significant effects of neutron irradiation on tensile properties of the composites were revealed, except the apparent UTS decrease for the HNLS composite irradiated below $\sim$610 °C (intermediate temperatures) to <3 dpa. According to the single filament tensile evaluation, fibers of both types retained the original strength during irradiation at intermediate temperatures but significantly deteriorated during bare fiber irradiations at high temperature ($\sim$910 °C). However, the fiber strength deterioration due to high temperature irradiation was not observed when irradiated in composite form. Combined results from the composite and single filament tensile tests, the hysteresis analysis, and the fracture surface examination, implied that the fiber–matrix interfacial frictional stress: (1) did not significantly change in the SA3 composite irradiated at intermediate temperatures, (2) obviously decreased in the HNLS composite during high temperature ($\sim$1000 °C) irradiation, and (3) likely increased in the HNLS composite during intermediate temperature irradiation. It remains unclear whether the apparent UTS decrease for the HNLS composite is genuinely an effect of neutron irradiation, however if so, one possible explanation is due to the differences in irradiation response between the fiber and the matrix.

Acknowledgements

This work was supported by the Office of Nuclear Energy, US Department of Energy under Contract DE-AC05-00OR22725 with UT-Battelle, LLC. Additional support was provided by the Knolls Atomic Power Laboratory. The authors would like to gratefully acknowledge contributions from R. Northey, D. Peters, and W. Cuddy of the Knolls Atomic Power Laboratory. Part of irradiation for this work was carried out in the High Flux Isotope Reactor, a Basic Energy Science User Facility.

References

[1] R.J. Price, Nucl. Technol. 35 (1977) 320–336.
[2] L.L. Snead, T. Nozawa, Y. Katoh, T.S. Byun, S. Kondo, D.A. Petti, J. Nucl. Mater. 371 (2007) 329–377.
[3] Y. Katoh, L.L. Snead, C.H. Henager, A. Hasegawa, A. Kohyama, B. Riccardi, J.B.J. Hegeman, J. Nucl. Mater. 367–370 (2007) 659–671.
[4] R. Naslain, Compos. Sci. Technol. 64 (2004) 155–170.
[5] Y. Katoh, L.L. Snead, T. Nozawa, W.E. Windes, N.B. Morley, Adv. Sci. Technol. 45 (2006) 1915–1924.
[6] M. Konomura, T. Mizuno, T. Saigusa, Y. Ohkubo, A promising gas-cooled fast reactor concept and its R&D plan, in: GLOBAL 2003, New Orleans, 2003.
[7] C. Forsberg, Fuel geometry options for salt-cooled advanced high-temperature reactors, in: ICAPP 2007, Nice, France, 2007.
[8] T. Hinoki, Y. Katoh, A. Kohyama, Mater. Trans. 43 (2002) 617–621.
[9] L.L. Snead, Y. Katoh, A. Kohyama, J.L. Bailey, N.L. Vaughn, R.A. Lowden, J. Nucl. Mater. 283–287 (2000) 551–555.
[10] T. Hinoki, L.L. Snead, Y. Katoh, A. Hasegawa, T. Nozawa, A. Kohyama, J. Nucl. Mater. 307 (2002) 1157–1162.
[11] Y. Katoh, T. Nozawa, L.L. Snead, T. Hinoki, J. Nucl. Mater. 367–370 (2007) 774–779.
[12] K. Ozawa, T. Nozawa, Y. Katoh, T. Hinoki, A. Kohyama, J. Nucl. Mater. 367–370 (2007) 713–718.
[13] G.A. Newsome, L.L. Snead, T. Hinoki, Y. Katoh, D. Peters, J. Nucl. Mater. 371 (2007) 76–89.
[14] T. Nozawa, Y. Katoh, A. Kohyama, Mater. Trans. 46 (2005) 543–551.
[15] T. Nozawa, E. Lara-Curzio, Y. Katoh, R.J. Shinavski, Tensile properties of advanced SiC/SiC composites for nuclear control rod applications, in: E. Lara-Curzio (Ed.), Mechanical Properties and Performance of Engineering Ceramics and Composites III, Wiley, 2007, pp. 223–234.
[16] L.L. Snead, Y. Katoh, S. Connery, J. Nucl. Mater. 367–370 (2007) 677–684.
[17] Y. Katoh, T. Nozawa, L.L. Snead, T. Hinoki, A. Kohyama, Fusion Eng. Des. 81 (2006) 937–944.
[18] T. Nozawa, Y. Katoh, L.L. Snead, T. Hinoki, A. Kohyama, Ceram. Eng. Sci. Proc. 26 (2005) 311–318.
[19] A.G. Evans, J.-M. Domergue, E. Vagaggini, J. Am. Ceram. Soc. 77 (1994) 1425–1435.
[20] Y. Katoh, L.L. Snead, T. Nozawa, T. Hinoki, A. Kohyama, N. Igawa, T. Taguchi, Mater. Trans. 46 (2005) 527–535.
[21] Y. Katoh, T. Nozawa, L.L. Snead, J. Am. Ceram. Soc. 88 (2005) 3088–3095.
[22] T. Nozawa, T. Hinoki, L.L. Snead, Y. Katoh, A. Kohyama, J. Nucl. Mater. 329–33 (2004) 544–548.
[23] J. Li, L.J. Porter, S. Yip, J. Nucl. Mater. 255 (1998) 139–152.
[24] T. Bus, Fundamental properties of point defects and small clusters in 3C-SiC: a combined molecular dynamics and experimental study, in: Department of Nuclear Engineering, University of California, Berkeley, California, 2006.
[25] M. Bockstedte, A. Mattausch, O. Pankratov, Phys. Rev. B 68 (2003) 205201.
[26] Y. Katoh, N. Hashimoto, S. Kondo, L.L. Snead, A. Kohyama, J. Nucl. Mater. 351 (2006) 228–240.
[27] L.L. Snead, S.J. Zinkle, D.P. White, J. Nucl. Mater. 340 (2005) 187–202.
[28] Y. Katoh, L.L. Snead, J. ASTM. Int. 2 (2005) 12377.
[29] T. Suzuki, T. Yano, T. Mori, H. Miyazaki, T. Iseki, Fusion Technol. 27 (1995) 314–325.
[30] J. Tersoff, Phys Rev B 39 (1989) 5566–5568.
[31] G.N. Morscher, M. Singh, J.D. Kiser, M. Freedman, R. Bhatt, Compos. Sci. Technol. 67 (2007) 1009–1017.
[32] Z.C. Xia, J.W. Hutchinson, Acta Metall. Mater. 42 (1994) 1933–1945.
[33] C.H. Hsueh, J. Mater. Sci. 30 (1995) 1781–1789.
[34] W.A. Curtin, J. Am. Ceram. Soc. 74 (1991) 2837–2845.
[35] M. Steen, J.L. Valles, ASTM Spec. Tech. Publ. 1309 (1997) 49–65.
[36] J.W. Hutchinson, H.M. Jensen, Mech. Mater. 9 (1990) 139–163.

[37] M.Y. He, B.-X. Wu, A.G. Evans, J.W. Hutchinson, Mech. Mater. 18 (1994) 213–229.
[38] C.H. Hsueh, Mater. Sci. Eng. A 161 (1993) L1–L6.
[39] T. Nozawa, Y. Katoh, L.L. Snead, J. Nucl. Mater. 367–370 (2007) 685–691.
[40] B.T. Kelly, J. Vac. Sci. Technol., A 4 (1986) 1171–1178.
[41] T.D. Burchell, Fission reactor applications of carbon, in: T.D. Burchell (Ed.), Carbon Materials for Advanced Technologies, Elsevier Science Ltd., Oxford, 1999, pp. 429–484.